Article

Low-Pressure Measurement Using an Extrinsic Fiber-Based Fabry-Perot Interferometer for Industrial Applications

Phairin Thaisongkroh[1], Saroj Pullteap[1],*, and Han Cheng Seat[2]

1 Department of Mechanical Engineering, Faculty of Engineering and Industrial Technology, Silpakorn University, Nakhon Pathom, Thailand
2 LAAS-CNRS, Université de Toulouse, CNRS, INP, Toulouse, France
*E-mail: saroj@su.ac.th (Corresponding author)

Abstract. The development of an extrinsic fiber-based Fabry-Perot interferometer (EFFPI) for low-pressure measurement in the industry applications has been studied in this work. Monochromatic light from a laser diode with a wavelength of 1310 nm is operated as a source for illuminating the EFFPI sensor. A 30 mm diameter PVC pipe is utilized as a target, of which one end is sealed with a rubber balloon and the end is connected to the air pressure flow controlling system. Furthermore, the center point of the balloon is secured with a reflective thin film, which has a reflectance of ~55%. For the performance validation of the fiber sensor, a low-pressure range from 5 to 50 mBar is released onto the target. With 12 rounds repeatability, the experimental results reported that the average measured pressure values from the EFFPI sensor are $4.915 - 50.988$ mBar. When compared to the reference instrument, the maximum and average errors in percentage terms are, however, 3.77% and 1.45%, respectively. In addition, results showed that the measured pressure value is directly proportional to the number of interference fringes, giving a sensitivity in the pressure measurement of the EFFPI sensor of 0.248 mBar/fringe.

Keywords: Low-pressure measurement, extrinsic fiber-based Fabry-Perot interferometer, rubber balloon, reflective thin film, fringe counting technique.

This article is based on the presentation at the International Conference on Engineering and Industrial Technology (ICEIT 2020) in Chonburi, Thailand, 11th-13th September 2020.

1. Introduction

Pressure measuring instruments are an important tool for several industries, especially in low-pressure measurement applications [1]. The classification of pressure can generally be divided into 3 main levels: low pressure (0 ≤ 10 kPa), regular pressure (>10 kPa ≤1 MPa) and high pressure (≥1 MPa) respectively [2] This is, in particular, due to the increasing demand from automotive manufacturing, air conditioning sector, oil and gas production, power plants, and also agriculture industries, etc. [3]. The numerous processes in these industries require precise pressure measurement and control in order to not exceed the determined limit of each industry [4]. However, existing instruments still incur high prices when compared to their relative accuracy, precision, and also sensitivity. Fiber optic sensors (FOS) are considered highly suitable tools for low-pressure measurement applications [5] where their high sensitivity, small size, lightweight, immunity to electromagnetic interference, operability in hazardous areas, and ability to be operated in difficult to access environments offer major advantages over conventional technologies [6]-[9]. For example, Qi *et al.* [10] have developed an extrinsic fiber-based Fabry-Perot interferometer (EFFPI) sensor coupled to the micro-electromechanical systems (MEMS) for very high-pressure measurement applications. The MEMS component was embedded into a glass capsule for validating the performance of the fiber sensor for measurable pressure between 2 - 120 MPa with an error of 0.079%. Meanwhile, Wang [11] has also developed an EFFPI sensor with a sensitivity of 137 mV/Pa in the frequency range from 84 Hz to 2.5 kHz to detect the flow rate of acetylene at atmospheric pressure. The results suggested that the developed system has the ability to detect acetylene flow rate as low as 1.5 ppb in chemical concentration, a value which is better than the industrial requirement for inspections of acetylene at 5 ppm. In addition, Bae [12] applied the Fabry-Perot interferometer (FPI), with 80 μm of core diameter, as a small size pressure instrument. This sensor is fabricated using a fiber Bragg grating (FBG), UV-curable polymer, and reflective layers for very low pressure measurements. Experimental results indicated a high linearity from the fiber sensor in the pressure range of 1.9 to 7.9 psi and a sensitivity of 94.34 psi/μm. This implies that the sensor can potentially be utilized in medical applications, with its small size and cost-effectiveness. Furthermore, Duraibabu [13] has developed an EFPI sensor, comprising an FBG, a hollow capillary fiber, and a reflective diaphragm, to allow underwater pressure measurement applications. The sensor is later implemented onto a remotely operated vehicle (ROV) for measuring underwater pressure and temperature. Results found that the developed sensor has stability when compared with the reference instrument, and could thus be utilized in the underwater measurement applications.

In this work, the design and development of an EFFPI sensor for low-pressure measurement applications is studied. Its operation implements the principle of fringe counting technique as a function of the deformation of material as the mechanism for the demodulation of the number of fringes into the pressure value. The expected results are the capability to measure pressure in the range of 0 to 50 mBar.

2. Related Theory

2.1. Extrinsic Fiber-Based Fabry-Perot Interferometer

It is considered to be 1 of the 4 types of optical fiber interferometers, which has several distinctive points as mentioned in the previous section. The extrinsic fiber-based Fabry-Perot interferometer (EFFPI) has been widely used in industrial applications especially [14] for high precision measurement. This is due to its simplicity, ease of implementation, and operability in hazardous environments [15]. Nowadays, the EFFPI has been adopted in the petrochemical industry, industrial safety, and also wind tunnel testing, etc. [9] A classical configuration of the EFFPI for high precision measurement is shown in Fig. 1.
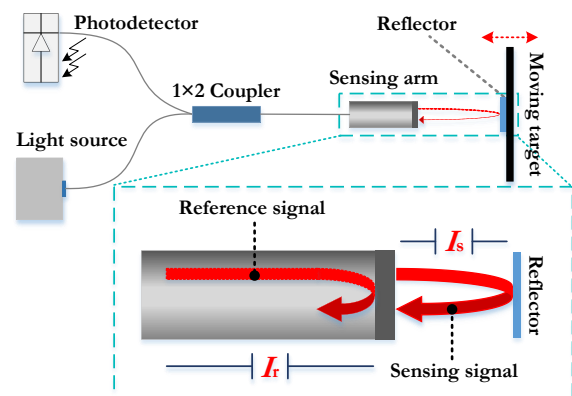

Fig. 1. Basic configuration of EFFPI sensor.

Monochromatic light wave from a laser diode source is injected into a 1x2 fiber coupler before propagation to the sensing arm. Approximately 4% of the light is reflected at the fiber end, referred to as the *"Reference signal* (I_r)*"*. Meanwhile, the remaining light is transmitted to the moving target mounted with a reflector, and next propagated into the sensing arm once more through back reflection. This signal is the *"Sensing signal* (I_s)*"* Consequently, the two signals superposition such that there is an optical phase difference leading to an *"Interference signal* (*I*)*"* with a given optical intensity [10], [16]:

$$I = I_s + I_r + 2\sqrt{I_s I_r}\cos(\varphi) \qquad (1)$$

when I_s is the intensity of the sensing signal
I_r is the intensity of the reference signal
φ is the optical phase difference between couple signals

From (1), the intensity of the interference fringe is determined by superposition of the intensity of I_s and I_r.

The resulting optical phase difference (φ) for a sensing cavity with refractive index n ($n = 1$ in air) and λ as the interrogating wavelength can be expressed as follows [3], [8], [10]:

$$\varphi = \frac{4\pi nD}{\lambda} \qquad (2)$$

Therefore, the displacement value (D) can thus be related to the number of fringes (N) detected in a given waveform period by

$$D = N\frac{\lambda}{2} \qquad (3)$$

2.2. Deformation of Material

The process involved causes the testing material to change in size, shape, and structure when external forces are exerted on the object, for example, tensile, compression, and shear force, etc [17]. The proposed process is applied to determine the thickness, resistance, strain, and stress of the material, as well as the modulus of material, etc. The characteristics of force exertion on the considered object is illustrated by Fig. 2.
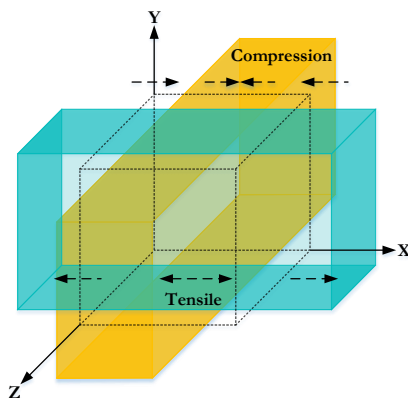

Fig. 2. Directional characteristics of force exertion on test material.

The subsequent stress induced is a function of the material internal resistance to the external force exerted onto a particular area. The induced strain is, on the other hand, the ration of the change in the material size to its original dimension [18] The stress (σ) is consequently defined by:

$$\sigma = \lim_{\Delta A \to 0} \frac{\Delta F}{\Delta A} \qquad (4)$$

where: ΔF is the tensile force in the material axis
ΔA is the cross-sectional area of the material perpendicular to the tensile force vector

The change of the material strain (ε) is correlated to the displacement (D) of the desired object [19] and can be calculated mathematically using (5).

$$\varepsilon = \frac{\Delta d}{L} \qquad (5)$$

where Δd is the change in the displacement of the test material and L indicates its initial dimension (e.g. length).

Additionally, the modulus elasticity (E) of the deformable test material can be used to find its resistance before rupture through the stress-strain relation given by [20]:

$$\mathrm{E} = \frac{Stress}{Strain} \Rightarrow \frac{\sigma}{\varepsilon} \qquad (6)$$

Furthermore, Poisson's ratio (υ), which is the ratio of the horizontal strain (ε_x) to the vertical strain (ε_y), can next be found using [21]:

$$\upsilon = \frac{\Delta x / x_0}{\Delta y / y_0} \Rightarrow \frac{\varepsilon_x}{\varepsilon_y} \qquad (7)$$

where: Δx is the change in horizontal length upon stretching
x_0 is the initial horizontal length
Δy is the change in vertical length upon stretching
y_0 is the initial vertical length

2.3. Optical Pressure Measurement

Pressure can be exerted in various forms: solid, liquid, or gas substances and so on, by considering the amount of force (F) applied in a perpendicular direction onto a given area (A), given by pascal (Pa) or kilopascal (kPa), which is equivalent to 1 newton per square meter (N/m²). It can also be expressed in units of pounds per square inch (psi) or milliBar (mBar). Regardless, its calculation is generally given as:

$$P = \frac{F}{A} \qquad (8)$$

The pressure value is still an all-important parameter for indicating the measurement of atmospheric, fluid, and gas pressure within the manufacturing processes of various industries, for example in pipeline fluid pressure control, steam pressure measurement in power plants, etc [22]. High-resolution pressure instruments are mostly developed based on optical devices [23]. From this perspective, FOSs are another set of tools that can be applied for gas, solid, and liquid detections [23]-[24], as well as for the simultaneous measurement of temperature, pressure, and also refractive index [25]-[26]. The configurations of the sensing element are generally different depending on the measurement applications. Nonetheless, an example of the precision pressure sensor using an optical fiber sensor can be illustrated by Fig. 3.
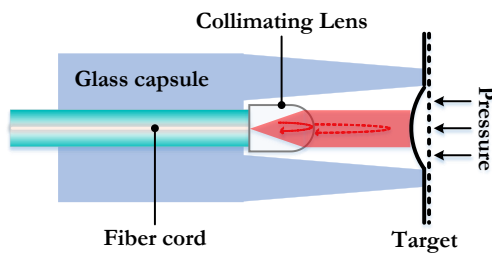
Fig. 3. Example of an optical fiber sensor applied for pressure measurement [27].

Here, a single-mode fiber (SMF) is spliced to a collimating lens which acts similarly to an optical concentrator, causing the input light to become a parallel output beam. Furthermore, the glass capsule (or capillary) is utilized as a cover jacket for controlling the direction of the light and protecting the optical devices against environmental effects. Thus, when pressures are exerted onto the measuring system, the target will be deformed, which proportionally corresponds to the variation of the target displacement (Δd) with the amount of the pressure change [27]. The relationship between these two variables is given by [28]:

$$P = \frac{16 \mathrm{E} h^3 \Delta d}{3 r^4 \left(1 - \upsilon^2\right)} \qquad (9)$$

when
- E   is the modulus of elasticity of material
- h is the material thickness
- Δd is the change in displacement
- r is the deformation radius of material
- υ is the Poisson's ratio

3. Experimental Setup

The workflow adopted in the design and development of the EFFPI for the low-pressure measurement is illustrated in Fig. 4.
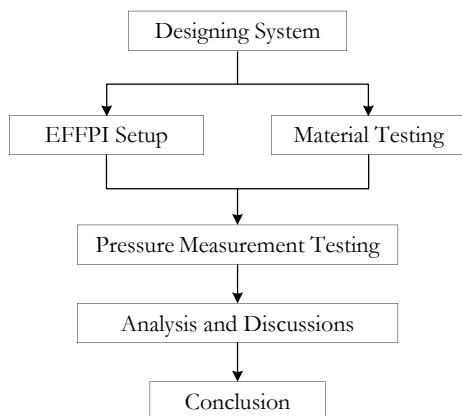

Fig. 4. Workflow of EFFPI development for low-pressure measurement.

3.1. Designing of EFFPI Measuring System

The EFFPI measuring system for low-pressure measurement is configured accordingly in Fig. 5.
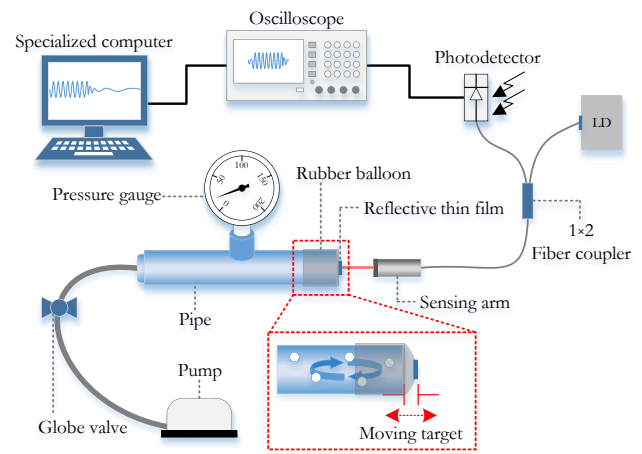

Fig. 5. Configuration of EFFPI measuring system for low-pressure measurement.

From the figure, a monochromatic wavelength of 1310 nm from the laser diode (LD) source is injected into a 1x2 fiber coupler and propagated to the sensing arm. Approximately 96% of the light beam is further transmitted to the moving target, which is sealed by the rubber balloon with a diameter and thickness of 30 and 0.35 mm, respectively. A reflective thin film with a reflectance value (R) of ~55% is secured to the center axis of the rubber balloon. The deformation of the rubber balloon is controlled by a pump and a globe valve respectively, wherein the deformation value is directly proportional to the air pressure and also displacement that is input into the system. A photodetector (*Thorlabs PDA10CS-EC*) is utilized at the output arm of the fiber coupler for receiving the interference signal and transducing into the electrical signal before transfer to a digital oscilloscope (*Tektronix TDS2014B*) for display and recording. The signal is next demodulated and analyzed by using an engineering application software on the dedicated computer. In general, interference signal will be generated when there is displacement within the system. The number of fringes is then counted and demodulated into the equivalent displacement value via the fringe counting technique, as demonstrated in (3) from which the pressure (*P*) is finally extracted according to (9) through the application software. In addition, a standard pressure gauge (*WIKA model 631*) is employed as a reference instrument for determining the measurement error as well as the performance of the fiber interferometer.

For the performance evaluation of the EFFPI sensor, the pressure in the range of 0 - 50 mBar, with an increasing interval of 5 mBar, is input into the system by adjusting the control valve. The measurement process is repeated over 12 times and the experimental results are recorded for further analysis.

3.2. Material Testing

This experiment involves the testing of the rubber balloon by using the tensile testing machine (*INSTRON model 5960 Series*), which is the method for defining the elasticity of the material via the pulling force at the steady-

state. The tensile force is recorded according to the deformation of the material. The testing exploits 10 samples of the material which are pulled until they are torn apart. The tensile resistance of the material is found to correspond to the maximum pulling force which it can withstand before rupture [29]. The material testing process is illustrated in Fig. 6.
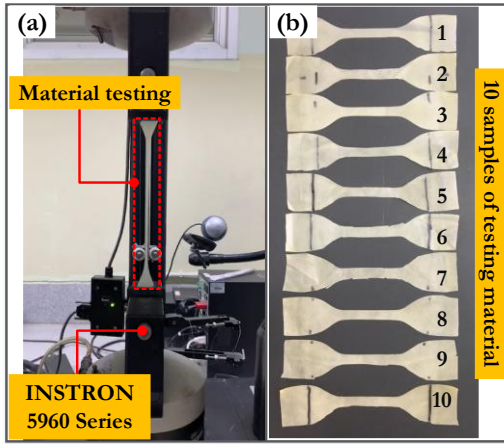

Fig. 6. Examples of material elasticity testing of rubber balloon; (a) material testing by using tensile machine; (b) 10 samples of tested rubber balloon.

The results from the material testing phase are analyzed in the form of a line graph. This indicates the relationship between the tensile stress and the tensile strain, or in other words, the *"Secant modulus"* of the tested material, which is plotted in Fig. 7.
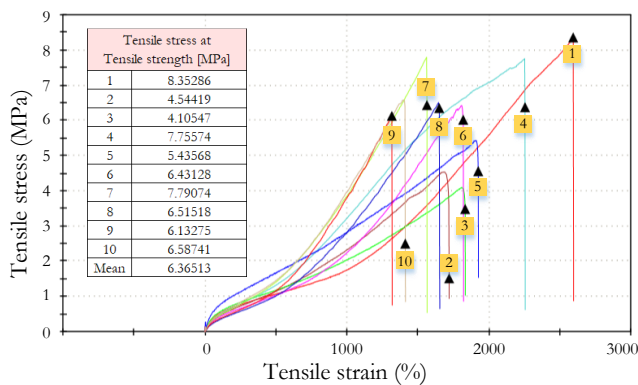

Fig. 7. Testing results obtained from tensile machine.

From the graph, it could be seen that the 10 material samples have an average tensile strength at break of 5.18%, whereas their average strain that resists the pulling force is approximately 6.365 MPa. Furthermore, upon completion of the material standard testing, the associated application software of the tensile testing machine calculates the related parameters of the testing material, as summarized in Table 1.

Table 1. Output parameters obtained from tensile machine in average value.

Symbol	Values	Description
E	6.36 MPa	Elasticity modulus of material
h	0.35 mm	Thickness of material
υ	4.9	Poisson's ratio of material
λ	1310	Wavelength
r	15 mm	Bending radius

These data are then used for calculating the pressure value as described in (9).

4. Experimental Results and Discussion

The experimental set-up of the EFFPI system for the low-pressure measurement is illustrated accordingly in Fig. 8 and 9, respectively.
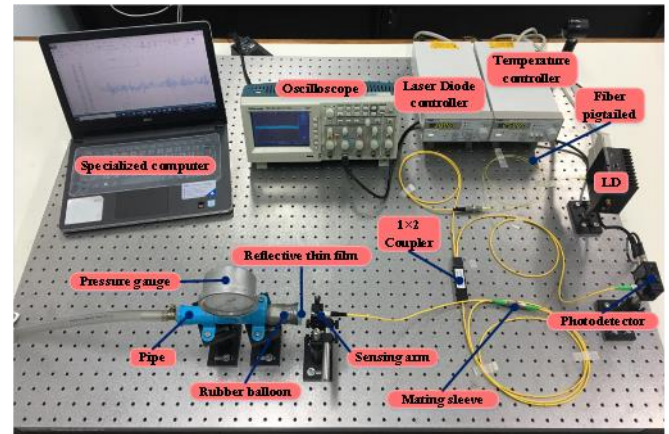

Fig. 8. Experimental setup of EFFPI system for low-pressure measurement application.
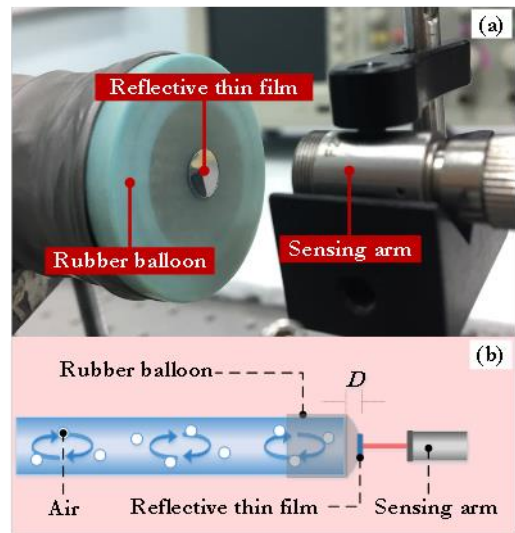

Fig. 9. Schematic of; (a) sensing arm and rubber balloon positioning; (b) airflow directions in target system.

The figures show the details of the experimental setup in this work. Figure 9 illustrates the installation of the reflective thin film, which is aligned with the sensing arm in parallel for maximizing its reflectance. For an air pressure of 1 mBar into the system, the output signal of the EFFPI sensor is detected and displayed on the oscilloscope, as shown in Fig. 10.
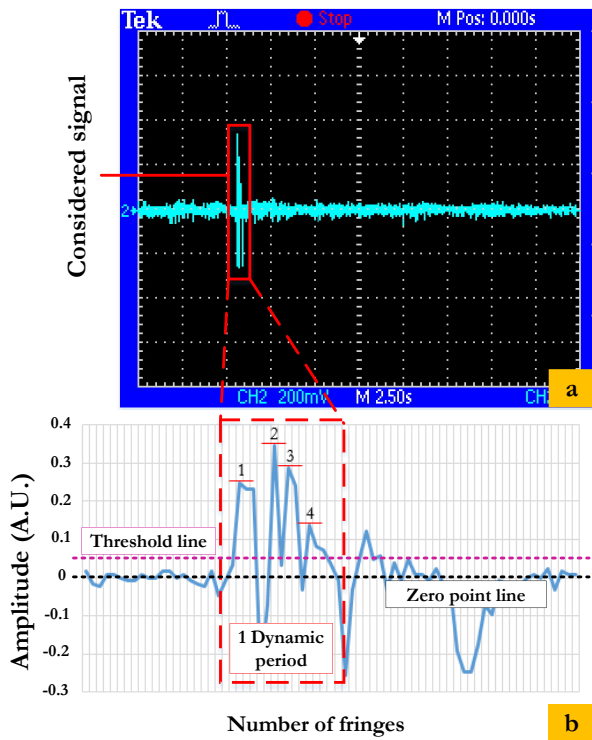
Fig. 10. Output signal obtained from EFFPI sensor; (a) interference signal displayed on oscilloscope and (b) number of fringes via engineering application software.

From Fig. 10(a), the output interference signal from EFFPI indicates the pressure exerted on the rubber balloon. The detected interference signal processed by the engineering application software (EAS) to automatically counting the number of fringes. To clarify, the signal peaks that exceeds the threshold value, over a zero point line by 15%, are counted. In addition, the fringes of a dynamic period in which the air instantaneously enters into the system are only considered. As demonstrated in Fig. 10(b), it is found that the input pressure of this demonstration corresponds to the output interference signal of four fringes/period. The displacement (D) calculation using (3) then gives the measured value to be approximately 2.62 µm. Moreover, by further applying (9), a demodulated pressure of 0.9912 mBar, with a percentage measurement error of 0.88%, respectively, have thus been occurred.

The results from both systems, that is the reference sensor and the EFFPI system, are consequently reported in Table 2

Table 2. Average experimental results from both types of pressure instruments.

Pressure from reference (mBar)	Average of number of fringe (N)	Pressure from EFFPI (mBar)	%Error
5	19.833	4.915	1.70
10	38.833	9.623	3.77
15	60.167	14.910	0.60
20	81.917	20.300	1.50
25	102.583	25.422	1.69
30	122.583	30.378	1.26
35	140.917	34.922	0.22
40	162.417	40.249	0.62
45	183.750	45.536	1.19
50	205.750	50.988	1.98

Data from Table 2 are next plotted in Fig. 11 to demonstrate the relationship between the number of fringes and the pressure value obtained by both sensors (P_{sens}) and (P_{ref}).
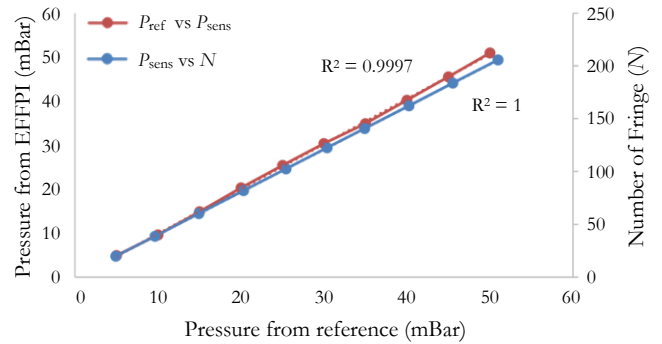

Fig. 11. Comparison of pressure between EFFPI and reference sensor versus number of fringes.

From the above graph, it is seen that the number of fringes has a significant linear relationship with the measured pressure from both instruments Likewise, the pressure values measured by using the EFFPI and the reference sensors illustrate a relatively high linearity. The aforementioned experimental results consequently prove that the EFFPI sensor is highly suitable for high-precision low-pressure measurement applications. From these results, the sensitivity of the EFFPI sensor is also estimated to be ~0.248 mBar/fringe. However, when this is compared to [12], the sensitivity value is exploited of 0.00549 psi/µm according to the demodulation fringe-counting technique mentioned in (3). This implies that the EFFPI in this experiment could provide more sensitivity in low-pressure measurements as compared to the reference work. Finally, the measurement errors of the proposed system in the experimented pressure range are analyzed and plotted in percentage form in Fig. 12.
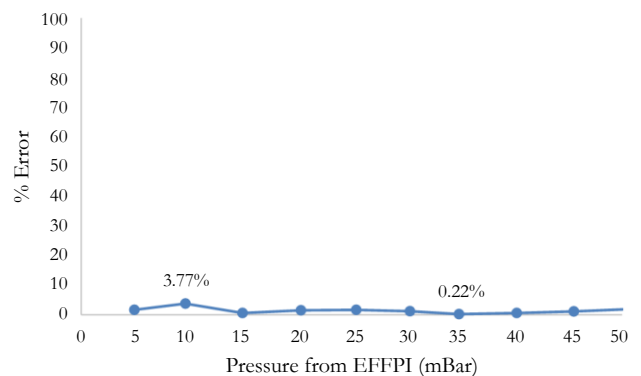

Fig. 12. Errors (in percent) from experimental results.

Over the pressure range of $0 - 50$ mBar (12 times repeatability), the maximum and minimum errors (in %) from the EFFPI sensor, as compared with the standard pressure gauge, correspond to 3.77% and 0.22%, respectively, while the average error obtained is ~1.45%. This error analysis thus strongly suggests that the proposed pressure instrument can accurately perform in real low-pressure applications. In comparison, the output data from the reference pressure gauge exhibit results that only indicate the integer values. The indicator on the scale would then have to be evaluated by the user. This could subsequently result in non-repeatability interpretation by the user and hence lead to low accuracy in the measurement readout. The EFFPI sensor, on the other hand, displays the output value in decimal number, implying that this sensor has a higher resolution than the standard instrument employed in the experiment. Therefore, the estimated error in the experiment might be due to the potential inaccuracy of the reference instrument. Additionally, environmental effects acting on the baseline parameters of the EFFPI sensor (e.g. temperature and, hence, wavelength variations, signal amplitude variation, parasite pressure variation, etc. might also incur some measurement errors. Last, but not least, slight vibrations from external sources might also perturb the measured number of fringes, consequently introducing some errors during interference signal demodulation.

5. Conclusion

The development of the extrinsic fiber-based Fabry-Perot interferometer (EFFPI) for the low-pressure measurement has been investigated using the principle of the fringe counting technique to detect the deformation of material which is subsequently demodulated into the desired pressure value. A reflective thin film, which is secured onto the rubber balloon at the center point of the sensing material, is utilized to create the sensing signal. The experimental results obtained from the EFFPI sensor, over an input pressure range of $0 - 50$ mBar, found comparatively similar pressure measurements of $4.915 - 50.988$ mBar, with an average percentage error of 1.45%. These results demonstrate that the EFFPI sensor is capable of low-pressure measurement applications. Moreover, the sensitivity of the EFFPI sensor system, through the fringe counting technique, is found to be ~0.248 mBar/fringe. This sensor is highly suitable for applications in the manufacturing industries, in particular for mechatronic engineering applications.

Acknowledgment

References

[1] X. Yeng *et al.,* "Electrospun Ionic Nanofiber Membrane-Based Fast and Highly Sensitive Capacitive Pressure Sensor," *IEEE Access*, vol. 7, pp. 139984-139993, 2019.

[2] E. Vorathin *et al.,* "Review of high sensitivity fibre-optic pressure sensors for low pressure sensing," *Opt Laser Technol.*, vol. 121, p. 105841, 2020.

[3] Z. Xinlei *et al.,* "Fiber-optic Fabry–Perot pressure sensor for down-hole application," *Opt Lasers Eng.*, vol. 121, pp. 289-299, 2019.

[4] C. Li *et al.,* "Design fabrication and characterization of an annularly grooved membrane combined with rood beam piezoresistive pressure sensor for low pressure measurements," *Sens. Actuator A Phys*, vol. 279, pp. 525-536, 2018.

[5] W. Ni *et al.,* "Highly sensitive optical fiber curvature and acoustic sensor based on thin core ultralong period fiber grating," *IEEE Photonics J.*, vol. 9, no. 2, p. 7100909, 2017.

[6] D. D. Vo *et al.,* "Measurement of low-pressure Knudsen force with deflection approximation for gas detection," *Results Phys.*, vol. 13, p. 102257, 2019.

[7] M. B. Gerdroodbary *et al.,* "Effect of Knudsen thermal force on the performance of low-pressure micro gas sensor," *Eur. Phys. J. Plus*, vol. 132, no. 7, 2017.

[8] J. Jiang *et al.,* "Noncontact ultrasonic detection in low-pressure carbon dioxide medium using high sensitivity fiber-optic fabry–perot sensor system," *J Lightwave Technol.*, vol. 35, no. 23, pp. 5079-5085, 2017.

[9] H. Liao *et al.,* "Phase demodulation of short-cavity Fabry–Perot interferometric acoustic sensors with two," *IEEE Photonics J.*, vol. 9, no. 2, 2017.

[10] X. Qi *et al.,* "Fiber optic Fabry-Perot pressure sensor with embedded MEMS micro-cavity for ultra-high pressure detection," *J Lightwave Technol.*, vol. 37, pp. 1-7, 2018.

[11] Q. Wang *et al.,* "A novel photoacoustic spectroscopy system using diaphragm based fiber Fabry-Perot sensor," *Procedia Eng*, vol. 15, pp. 5395-5399, 2011.

[12] H. Bae and M. Yu, "Miniature Fabry-Perot pressure sensor created by using UV-molding process with an optical fiber-based mold," *Opt. Express*, vol. 20, no. 13, pp. 14573-14583, 2012.

[13] D. B. Duraibabu *et al.,* "An optical fibre depth (pressure) sensor for remote operated vehicles in underwater applications," *J. Sens.*, vol. 17, no. 2, p. 406, 2017.

[14] T. Liu *et al.,* "Simultaneous measurement of pressure and temperature based on adjustable line scanning polarized low-coherence interferometry with compensation plate," *IEEE Photonics J.*, vol. 10, no.4, p. 7104109, 2018.

[15] C. Yu *et al.*, "Fitting algorithm for interferometric spectrum of fiber Fabry-Perot cavity acoustic sensors," *Conf. Ser.: Earth Environ. Sci.*, vol. 310, no. 032038, pp. 1-6, 2019.

[16] S. Pullteap, "Development of an optical fiber-based interferometer for strain measurements in non-destructive application," *Electr. Eng.*, vol. 99, pp. 379–386, 2017.

[17] A. Nie *et al.*, "Approaching diamond's theoretical elasticity and strength limits," *Nat. Commun.*, vol. 10, no. 5533, 2019.

[18] P. Kumar *et al.*, "An overview of stress-strain analysis for elasticity equations," in *Elasticity of Materials Basic Principles and Design of Structures*. London: IntechOpen, 2018, ch. 2, pp. 1-19.

[19] Z. Ma *et al.*, "Sensitivity-enhanced extrinsic Fabry–Perot interferometric fiber-optic microcavity strain sensor," *J. Sens.*, vol. 19, no. 19, p. 4097, 2019.

[20] C. Uff *et al.*, "Further characterization of changes in axial strain electrograms due to the presence of slippery tumor boundaries," *J. Med. Imaging*, vol. 5, no. 2, p. 021211, 2018.

[21] H. Belyadi *et al.*, "Rock mechanical properties and in situ stresses," in *Hydraulic Fracturing in Unconventional Reservoirs*, 2nd ed. Gulf Professional Publishing, 2019, ch. 13, pp. 215-231.

[22] Y. Zhao *et al.*, "Improving operational flexibility by regulating extraction steam of high-pressure heaters on a 660 MW supercritical coal-fired power plant: A dynamic simulation," *Appl Energ.*, vol. 212, pp. 1295-1309, 2018.

[23] L. Zhang *et al.*, "A high-speed second-order photonic differentiator based on two-stage silicon self-coupled optical waveguide," *IEEE Photonics J.*, vol. 6, no. 2, p. 7900505, 2014.

[24] B. Xu *et al.*, "Optical fiber Fabry–Perot interferometer based on an air cavity for gas pressure sensing," *Photonics Res.*, vol. 9, no. 2, 2017.

[25] S. Pevec and D. Donlagic, "Multiparameter fiber-optic sensor for simultaneous measurement of thermal conductivity, pressure, refractive index, and temperature," *IEEE Photonics J.*, vol. 9, no. 1, 2017.

[26] Y. Zhang *et al.*, "Simultaneous measurement of temperature and pressure with cascaded extrinsic Fabry–Perot interferometer and intrinsic Fabry–Perot interferometer sensors," *Opt. Eng*, vol. 53, no. 6, p. 067101, 2014.

[27] J. Eom *et al.*, "Fiber-optic Fabry–Perot pressure sensor based on lensed fiber and polymeric diaphragm," *Sens. Actuator A Phys.*, vol. 225, pp. 25-32, 2015.

[28] Y. Jiang *et al.*, "Fabrication of All-SiC Fiber-Optic Pressure Sensors for High-Temperature Applications," *J. Sens.*, vol. 16, no. 10, p. 1660, 2016.

[29] R. J. Schaefer, "Mechanical properties of rubber," in *Harris' Shock and Vibration Handbook*, 5th ed. New York: The McGraw-Hill Companies, 2001, ch. 33, pp. 33.1–33.18.

Phairin Thaisongkroh received the B.S. degrees in Software Engineering from the Nakhon Pathom Rajabhat University, Thailand, in 2014 and the M.Sc. degree in Management Information Systems from King Mongkut's University of Technology North Bangkok, Thailand, in 2018 respectively. She currently is studying Doctoral degree in energy engineering at the Silpakorn University, Thailand. Her research interests are the development of a fiber-optic sensor for biogas sensing applications.

Saroj Pullteap (Ph.D.) is, currently, an Associate Professor at the Department of Mechanical Engineering, Silpakorn University, Thailand. He received a Bachelor of Industrial Education in Computer Technology Program from the King Mongkut's Institute of Technology North Bangkok in 2002, and also a Master of Engineering in Industrial Metrology from the King Mongkut's University of Technology Thonburi in 2003. In 2007, he, consequently, received a Philosophy Doctor in Optoelectronics Engineering from the University of Toulouse, France. His research works are the development of a optical fiber sensor for mechatronics engineering and biomedical engineering applications.

Han Cheng Seat (Ph.D.) is an Associate Professor at the Department of Electronic Engineering & Signal Processing, Institut Nationale Polytechnique de Toulouse, France. He received first-class honor in Bachelor of Engineering (Mechanical Engineering) in 1996, and further Doctoral of Philosophy in Engineering from the University of Glasgow, the United Kingdom in 2001. His research interests are in the fields of fiber optic and photonic sensors, as well as geosciences, gas sensing, and metrology.